Characterisation of scintillator-based gamma spectrometers for determination of sample dose rate in OSL dating applications

Bu, Minqiang; Murray, Andrew Sean; Kook, Myungho; Helsted, Louise Maria; Buylaert, Jan-Pieter; Thomsen, Kristina Jørkov

Published in:
Radiation Measurements

Link to article, DOI:
10.1016/j.radmeas.2018.07.003

Publication date:
2018

Document Version
Publisher's PDF, also known as Version of record

Radiation Measurements 120 (2018) 253–259

Contents lists available at ScienceDirect

Radiation Measurements

journal homepage: www.elsevier.com/locate/radmeas

Characterisation of scintillator-based gamma spectrometers for determination of sample dose rate in OSL dating applications

Minqiang Bu[a,*], Andrew Sean Murray[b], Myungho Kook[a], Louise Maria Helsted[a], Jan-Pieter Buylaert[a,b], Kristina Jørkov Thomsen[a]

[a] Center for Nuclear Technologies, Technical University of Denmark, DTU Risø Campus, DK-4000, Roskilde, Denmark
[b] Nordic Laboratory for Luminescence Dating, Department of Geoscience, Aarhus University, Risø Campus, DK-4000, Roskilde, Denmark

ARTICLE INFO

Keywords:
NaI(Tl) detector
Scintillation gamma spectrometry
Spectrum drift correction
Dose rate measurement
OSL dating

ABSTRACT

A recent inter-comparison (Murray et al., 2015) has helped to highlight variability in the measurement of dose rate between luminescence laboratories. Part of this variability probably reflects the difficulties of homogenising and dissolving samples so that the < 500 mg used in e.g. ICP-MS and NAA is representative. High resolution gamma spectrometry is the obvious alternative because it can measure samples 100–1000 times larger, but the instrumentation is low-throughput, high capital and running cost, and requires skilled personnel to maintain operation over many years. Here we investigate the potential of traditional low-cost, low maintenance alternatives based on a 3" × 3" NaI(Tl) scintillation crystal. The temperature stability is investigated, and a linear (with intercept) correction for spectra drift based on the 1.46 MeV peak from ^{40}K and the ~100 keV composite X-ray peak from uranium and thorium is shown to minimise this problem. Using a calibration based on wax impregnated standards, the minimum detection limits (MDL) are 25 Bq/kg (^{40}K), 4.8 Bq/kg (^{238}U), 2.5 Bq/kg (^{232}Th) for 250–300 g of sample; systematic deviations around the expected values are also shown to be acceptable as the MDL is approached. Finally, we compare the activity concentrations and resulting dry dose rates derived from our NaI-based system with those from routine high resolution gamma spectrometry, and conclude that the new analytical facility is very suitable for accurate and precise dose rate determination.

1. Introduction

Low resolution gamma spectrometry was the laboratory technique of choice for many years, but more recently it has largely been relegated to field measurements, having almost completely been superseded by high resolution germanium-based detectors in the laboratory. Nevertheless, low resolution spectrometry remains much cheaper, requires less maintenance and labour, and, at least at high activity concentrations, is capable of accurate analyses. A recent inter-comparison (Murray et al., 2015) has helped to highlight variability in the measurement of dose rate between luminescence laboratories. Here we investigate whether low resolution spectrometry could provide analyses of natural activity concentrations of sufficient accuracy and precision for use in the dosimetry calculations in luminescence age determination.

It is well known that photomultiplier tubes (e.g. Plettner et al., 2011) and NaI(Tl) crystals are temperature sensitive (e.g. Moszynski et al., 2006). This causes gain drift and thus movement of the gamma spectrum during measurement. This temperature dependence must be compensated for before the spectra can be analysed further. Different methodologies have been applied to correct for drift in gamma spectra, either off-line (Casanovas et al., 2012; Mitra et al., 2016) or on-line using e.g. a separate ^{214}Am source (Marett et al., 1976), a ^{137}Cs reference source (Borg et al., 1985) or the ^{40}K signal present in the sample spectra (Qin et al., 2012).

Here we outline the results of using an off-line gain-correction method based on two widely spaced but ubiquitous peaks, the complex X-ray peak from uranium and thorium at ~100 keV and the 1.46 MeV gamma emission from ^{40}K. Experiments first investigate the dependence of peak position on temperature by counting a mixed ^{40}K, ^{238}U and ^{232}Th sample at different temperatures. Based on the results of these experiments, a drift correction algorithm is developed to correct the spectra from ^{40}K, ^{238}U and ^{232}Th calibration standards, background, and unknown samples to a uniform energy scale.

An improved three-energy-window approach is then used to analyse the drift-corrected spectra, to allow efficiency calibration and for derivation of activity concentrations in unknown samples. Minimum detection limits (MDL) are investigated, and the accuracy of the analyses

* Corresponding author.
E-mail address: mibu@dtu.dk (M. Bu).

https://doi.org/10.1016/j.radmeas.2018.07.003
Received 8 December 2017; Received in revised form 29 June 2018; Accepted 6 July 2018
Available online 07 July 2018

as the MDL is approached is discussed. Finally we calculate the ^{40}K, ^{238}U and ^{232}Th activity concentrations in 20 natural samples, previously analysed using high resolution gamma spectrometry, and compare the activity concentration analyses and the resulting dry dose rates.

2. Materials and methods

2.1. Experimental setup

The scintillator detector used in this paper is a 3" × 3" NaI(Tl) crystal (Harshaw) connected to a digital tube base (TB-5, Amptek) consisting of a digital pulse processor (DPP), a charge sensitive preamplifier, a multichannel analyzer (MCA), and power supplies (low voltage and high voltage). The detector and MCA are all contained within a 10 cm thick lead shield. The gamma spectra from NaI(Tl) detector were acquired with the DppMCA software from Amptek. DoseRateAnalyzer software (developed in-house based on MATLAB®) is used for drift corrections, ^{40}K, ^{238}U and ^{232}Th efficiency calibration, activity concentration analysis and dose rate calculation. In order to evaluate the performance of the NaI(Tl) detector and the accuracy of the algorithm we employ, the samples were also measured using our standard high resolution gamma facility (Murray et al. these proceedings). Because of the different detector dimensions, these required separately prepared samples for counting, but both the wax/sediment cups made for the NaI detector and those counted on the high resolution facility were made from the same homogenised sediment samples.

In order to investigate the relationship between temperature change and drift in spectrum peak positions, a temperature regulator was built around NaI(Tl) detector in the lead shield to control the temperature in the detector chamber. The experimental setup is illustrated in Fig. 1(a) and (b). Four sets of resistive heaters connected in series are positioned at the four corners of the detector chamber. Each heater is mounted on an aluminium heatsink equipped with an electric fan to circulate the heated air in the detector chamber. The detector chamber is surrounded by 5–8 cm of thermal insulation both inside and outside the lead shield to help keep the temperature of the sample and detector stable. During data collection, temperatures at the top surface of NaI(Tl) crystal, side surface of the heater, PMT and TB-5 digital tube base, and air surrounding the crystal were continuously measured by K-type thermocouples and monitored by a thermocouple data logger (USB TC-08, Pico Technology, UK). Only the temperature of the air between two heaters at position D, as illustrated in Fig. 1(b), was used as a feedback to control the temperature of the heater. This approach not only simplifies the temperature control algorithm, but also prevents the overheating of the whole system, especially the more vulnerable detector.

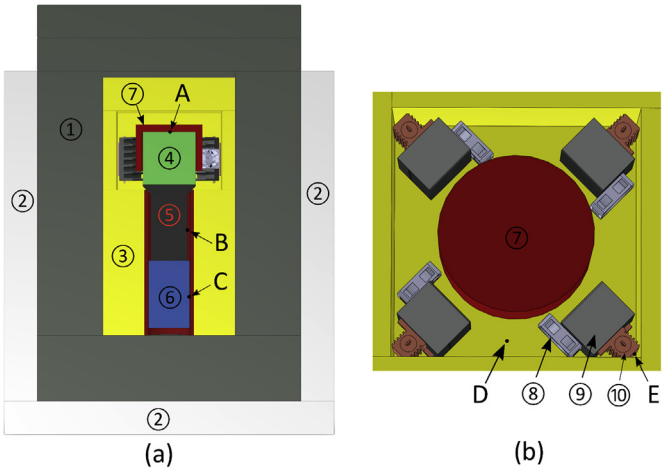

Fig. 1. (a) A cross-section of the detector in the lead shield. (b) A top view of the measurement chamber after removing the lead lid and top internal insulation layer. The setup includes 11 main components: ① - lead shield, ② - external insulation, ③ - internal insulation, ④ - NaI(Tl) detector, ⑤ - PMT, ⑥ - digital tube base (TB-5), ⑦ - sample cup, ⑧ - electric cooling fan, ⑨ - heat sink, ⑩ - resistive heater, and five temperature sensors (A–E) monitoring at five different positions.

Samples are ground to < 200 μm and mixed with high viscosity wax (Bottle wax, blend 1944, British Wax Refining Company) at a typical mass ratio of 1:2 (wax:sample), to give a typical sample mass of 250–300 g. Sample and calibration standards are cast in a cup-shaped geometry, with wall thickness 10 mm, internal diameter 80 mm and length 60 mm (Fig. 1(a)). When inverted, the cup fits over the top of the NaI detector. At the energies of interest, the dependence of self-attenuation on sample mass for all likely mixtures of wax:sample is < 2% (Murray et al. these proceedings).

Uranium and thorium calibration standards were prepared by diluting the appropriate certified reference material BL-5 (7.09 ± 0.03% U) (NRCAN-1) or OKA-2 (2.893 ± 0.058% Th) (NRCAN-2) in low activity quartz sand, then mixing with wax to give individual parent activities of ~800 Bq per cup. For potassium calibration standards, analytical grade K_2SO_4 (14.20 Bq/g assuming stoichiometry, purity given as 100.4%) was mixed directly with wax to give ~2700 Bq per cup. From calculation the expected uncertainties arising from weighing are < < 1%. Three standards were prepared from separate dilutions for each radionuclide. A background sample cup was prepared by casting pure wax. In addition, a mixed sample was prepared by diluting BL-5 and OKA-2 in K_2SO_4 to give a sample cup containing ~2700 Bq ^{40}K and ~70 Bq ^{238}U and ^{232}Th. The peaks of interest in the spectrum of this mixed sample cup were used as reference peaks for drift correction of all spectra from unknown samples and ^{40}K, ^{238}U and ^{232}Th calibration standards.

Note that our NaI(Tl) spectrometer is insensitive to the photons emitted by the first part of the ^{238}U series (all low energy and/or low intensity). It mainly detects photons emitted by ^{222}Rn short-lived daughters. One of the purposes of mixing the sample in wax is to fully retain all ^{222}Rn, so that after some period of storage (here typically > 20 days) ^{222}Rn and all short-lived daughters are in secular equilibrium with ^{226}Ra. The degree of secular equilibrium between ^{238}U and ^{226}Ra is in general unknown; in this study, we assume ^{226}Ra activity concentration equal to ^{238}U activity concentration. All uranium series analyses are therefore referred to as measurements of uranium.

2.2. Methodology

2.2.1. Peak area analysis: an improved three-window approach

We adopted and improved the standard three-window approach (e.g. Desbarats and Killeen, 1990) to calculate ^{40}K, U series and Th series (KUT) activities; these are shown as three vertical bands in Fig. 2, where spectra of the three calibration standards and a background spectrum are presented. In most KUT analyses using low resolution detectors, apart from measuring the 1.46 MeV ^{40}K peak, it is a standard practice to measure the 1.76 MeV ^{214}Bi line from the U series, and the 2.61 MeV line from ^{208}Tl in the Th series. This is because these high energy peaks are well separated and do not suffer from significant cross-contamination from the other spectra. Unfortunately, this is at the cost of sensitivity; a typical 3" × 3" cylindrical crystal is relatively insensitive to such high energy photons, and for small samples in laboratory analysis, the count rates are low. Here we have chosen rather to use the 239 keV line from ^{212}Pb (Th series) and 352 keV line from ^{214}Pb (U series) (together with the 1.46 MeV ^{40}K peak); these are two of the most intense peaks in the U series and Th series spectra (Fig. 2, lowest energy group). However, because of the relatively low resolution of a NaI(Tl) crystal, to obtain an accurate measurement of these closely spaced low energy gamma rays, precise correction for peak drift is of particular importance. This is discussed in detail in the next section.

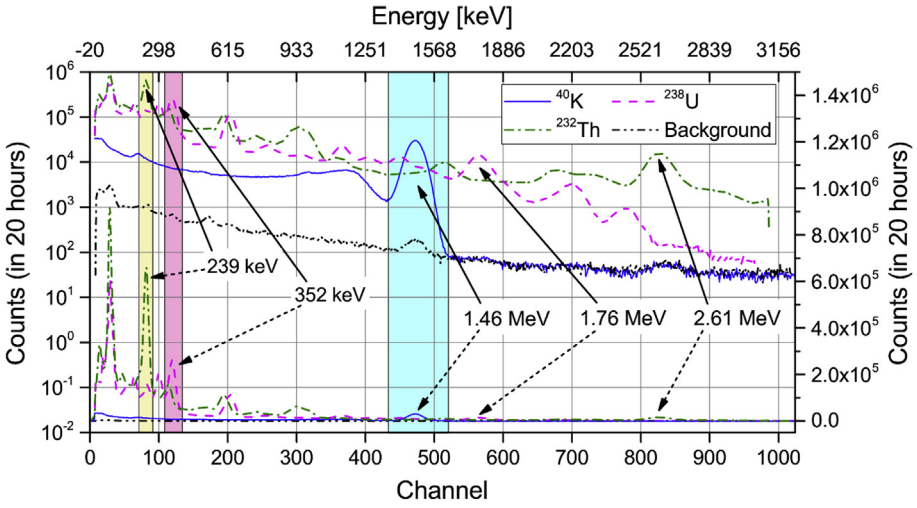

Fig. 2. Illustration of the improved three-window approach. Three shaded vertical bands counting from left to right, denote ^{232}Th, ^{238}U and ^{40}K energy windows of interest, respectively, for calculating the calibration constants. The spectra of ^{40}K, ^{238}U and ^{232}Th calibration standards and background are shown in both logarithmic scale (four top spectra, left y axis) and linear scale (four bottom spectra, right y axis). The spectra on the linear scale show the prominent 239 keV peak (^{212}Pb, Th series) and 352 keV peak (^{214}Pb, U series); compare with the intensities of the 2.61 MeV peak (^{208}Tl, Th series) and 1.76 MeV peak (^{214}Bi, U series).

2.2.2. Gamma spectra drift correction

In the development of a drift correction algorithm, the effect of the main factor controlling drift, temperature, must be characterised. In this study, all the spectra were collected first for a certain period (i.e. 20 h), and the drift correction algorithm was then applied to the final spectra.

Following Casanovas et al. (2012), for a given PMT high voltage and amplifier gain we make two assumptions concerning energy drift in our system:

(i) that the channel into which a pulse derived from a particular photon energy is counted is only dependent on the temperature, as described below.

$$C_{ik} = C_{i0} \times f_i(T_k), \ i = 1, \ 2..., \ 1024 \quad (1)$$

where C_{i0} and C_{ik} are the channel positions at temperature T_0 and T_k, respectively, and $f_i(T_k)$ is a ratio only dependent on temperature T_k. The total number of channels in this study is 1024.

(ii) that the relative channel displacement due to temperature change ΔT is same for all channels.

$$f_1(T_k) \approx f_2(T_k) \approx ... \approx f_{1024}(T_k) \approx f(T_k) \quad (2)$$

In order to evaluate the second assumption, the mixed ^{40}K, ^{238}U, ^{232}Th sample was measured at different fixed temperatures of 25, 30, 35, 40, 45 and 50 °C, respectively for 20 h. Each time the set temperature was changed to the next value (e.g. from 30 to 35 °C), we waited for another 20 h to allow the temperature in the whole system to reach thermal equilibrium before counting started. Fig. 3 shows the actual temperature variation (ΔT) on the top surface of the detector during 20 h of continuous counting at the various fixed temperatures. It appears that the temperature of the detector can be controlled to a $\Delta T \leq 0.4$ °C. Unsurprisingly, the maximum temperature change occurred at ~25 °C, when the heater was actually switched off and the temperature of the whole system was drifting below or above a nominal room temperature (e.g. 25 °C). With such a small temperature variation, five peaks of interest (identified in Fig. 2) have, from low to high energy, moved in 20 h by only 0.13, 0.12, 0.12, 0.12, and 0.12%, respectively.

The dependence of peak position on temperature for six different peaks is shown in Fig. 4. All data are well represented by straight lines and there is no significant dependence of slope on energy; over the entire energy range of interest the gain change ratio, represented by relative slopes (RS) of the fitted lines in Fig. 4, is −0.301 ± 0.004%/°C (n = 6) above room temperature, confirming the validity of the second assumption made above.

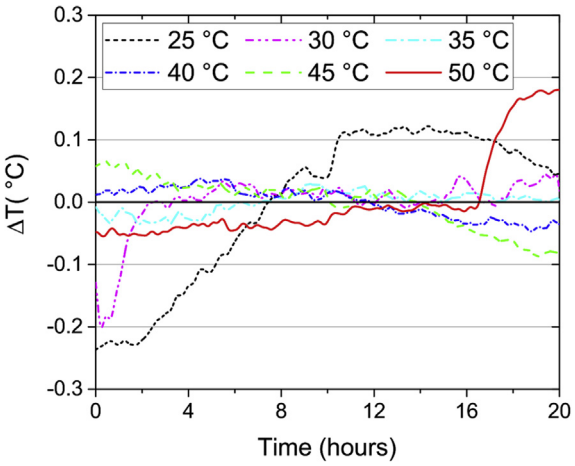

Fig. 3. Actual temperature changes ΔT on the NaI(Tl) detector over 20 h when held at a nominal 25, 30, 35, 40, 45 and 50 °C. For the 25 °C data set, the heater was in fact switched off and the system was equilibrated at room temperature.

We next test the accuracy with which a simple linear peak position correction can be undertaken. An intercept is included in this correction, to allow for the possibility that the MCA offset has not been exactly zeroed. First a reference spectrum was collected at a fixed temperature (T_0, 30 °C) using the mixed ^{40}K, ^{238}U, ^{232}Th sample (see above). In this reference spectrum, the positions of the composite X-ray peak at ~100 keV, and ^{40}K peak at 1.46 MeV were selected as reference peaks.

In general, the correction assumes a linear relationship with an intercept:

$$\begin{bmatrix} C_{Drifted\_p1} & 1 \\ C_{Drifted\_p2} & 1 \end{bmatrix} \begin{bmatrix} C_{ratio} \\ C_{intercept} \end{bmatrix} = \begin{bmatrix} C_{Ref\_p1} \\ C_{Ref\_p2} \end{bmatrix} \quad (3)$$

where $C_{Drifted\_p1}$ and $C_{Drifted\_p2}$ are the centroids of selected peaks in the drifted spectrum, while C_{Ref_p1} and C_{Ref_p2} are the centroids of corresponding peaks in the reference spectrum. C_{ratio} is the linear correction factor and $C_{intercept}$ is the intercept correction.

Finally the drifted channels are corrected by:

$$C_{i\_corrected} = C_{i\_drifted} \times C_{ratio} + C_{intercept}, \ i = 1, \ 2, \ ..., \ 1024 \quad (4)$$

where $C_{i\_drifted}$ are the original uncorrected channels and $C_{i\_corrected}$ are the corrected channels; the latter are fractional and are finally rounded to integer values.

With the corrected channels, the counts in each original channel $Count_{i\_Original}$ were interpolated into the corrected channel in the in-

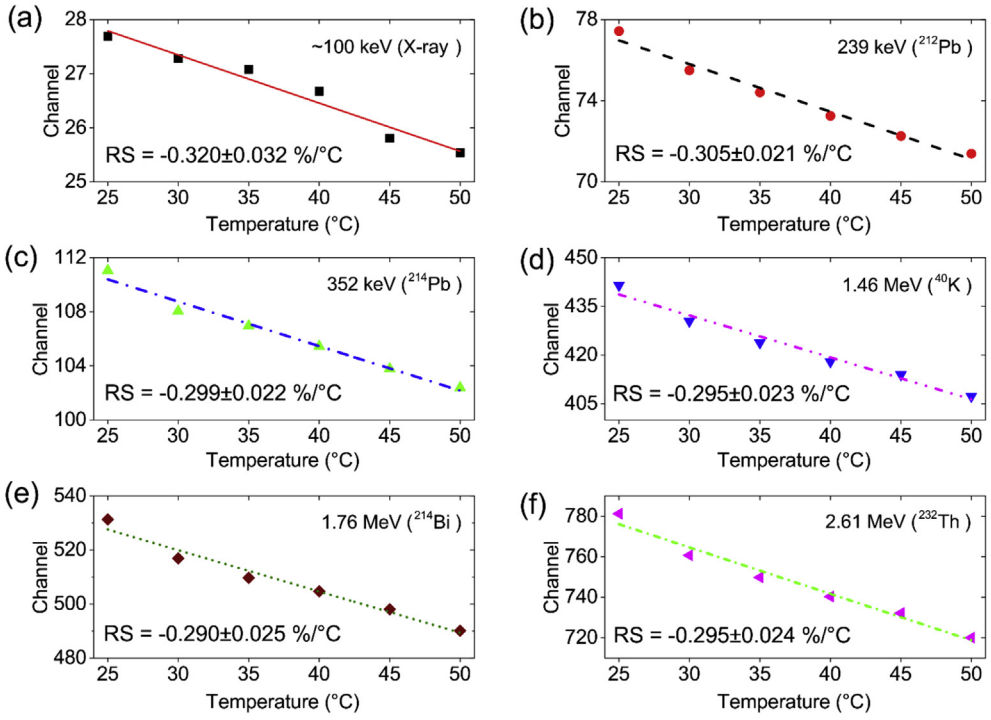

Fig. 4. Centroid positions of peaks of interest at different temperatures ranging from 25 to 50 °C, and linear fits to the data. The gain change ratios, i.e., the relative slopes (RS, %/°C) of the fitted data are shown in each panel.

house developed DoseRateAnalyzer software. During the drift correction, the spectrum is actually either compressed when $C_{ratio} < 1$ or expanded when $C_{ratio} > 1$, causing narrowing or broadening of peaks of interest, respectively. Therefore, the corrected counts $Count_{i\_Corrected}$ in the corrected channels are adjusted by dividing the counts in the original channels by C_{ratio}, to compensate the changing of the counts in each channel during drift correction. Therefore:

$$Count_{i\_Corrected} = Count_{i\_Original}/C_{ratio},\ i = 1,\ 2...,\ 1024 \quad (5)$$

Because the ^{40}K, ^{238}U and ^{232}Th calibration standards and unknown samples all have different characteristic peaks, selection of reference peaks is dependent on the spectrum to be drift corrected. For unknown samples containing ^{40}K, ^{238}U and ^{232}Th, drift correction employs the ubiquitous 100 keV (X-ray) and 1.46 MeV (^{40}K) emissions (this also applies to background spectra). This is not possible when correcting the gamma spectra from calibration standards; in the ^{40}K standard spectrum, the X-ray peak is not detectable, and so the 1.46 MeV (^{40}K) and the 2.61 MeV (Th series) peaks are used (the 2.61 MeV peak is present as a result of the high energy background contribution). For the ^{238}U calibration standard with negligible ^{40}K, we employ the X-ray peak and the ^{214}Bi peak (1.76 MeV, U series). Finally, for ^{232}Th calibration standard, we use the X-ray peak and the ^{208}Tl peak (2.61 MeV). This ensures that the peaks of interest, especially the 239 keV and 352 keV peaks from the ^{232}Th and ^{238}U series, are bracketed by the peaks used for drift correction.

3. Results and discussion

3.1. Drift correction results

Fig. 5 shows a series of gamma spectra (bottom group) measured using the mixed ^{40}K, ^{238}U, ^{232}Th sample with the temperature fixed at 25, 30, 35, 40, 45 and 50 °C. The peaks in the spectrum shift towards lower energies as the temperature increases. The positions of the two reference peaks at 100 keV (X-ray peak) and 1.46 MeV (^{40}K peak) were used to establish a linear correction factor with an intercept, resulting in corrected spectra shown in the stacked upper group of spectra in Fig. 5. The enlarged insets clearly show the accuracy of the algorithm used for spectra drift correction over the entire energy range of interest (from the X-ray peak to the Th series 2.61 MeV peak). It is also observed from Fig. 5 that there are some amplitude differences in the corrected spectra at higher energies, even though the peak position is aligned well. Fortunately this is negligible in the lower energy region where the peaks of interest are located.

3.2. Calibration and calculation of activity concentrations in unknown samples

The calibration standard cups were each counted for 20 h, drift corrected, corrected for the (negligible) background contribution, and the relevant count rates in the integration areas of interest are then derived from all spectra. These count rates were divided by the known sample activity concentrations and counting time (in ks), to give the calibration constants *Cc* in the three-window matrix:

$$Cc = [C_{cK}\ \ C_{cU}\ \ C_{cTh}] = \begin{bmatrix} K_K & U_K & Th_K \\ K_U & U_U & Th_U \\ K_{Th} & U_{Th} & Th_{Th} \end{bmatrix} \quad (6)$$

along with their uncertainties:

$$Un\_Cc = [Un\_C_{cK}\ \ Un\_C_{cU}\ \ Un\_C_{cTh}] = \begin{bmatrix} Un\_K_K & Un\_U_K & Un\_Th_K \\ Un\_K_U & Un\_U_U & Un\_Th_U \\ Un\_K_{Th} & Un\_U_{Th} & Un\_Th_{Th} \end{bmatrix} \quad (7)$$

To reduce the contribution from dilution/casting of the standards, three samples of each calibration standard, K1-3, U1-3 and Th1-3 were cast, counted and analysed. The individual coefficients in the *Cc* matrix were obtained by averaging three individual coefficients from three similiar calibration standards. For example, to obtain an average K_K, K_U and K_{Th}, the count rates from K1, K2 and K3 standards were calculated individually, using a single spectrum of ^{238}U and ^{232}Th. Then:

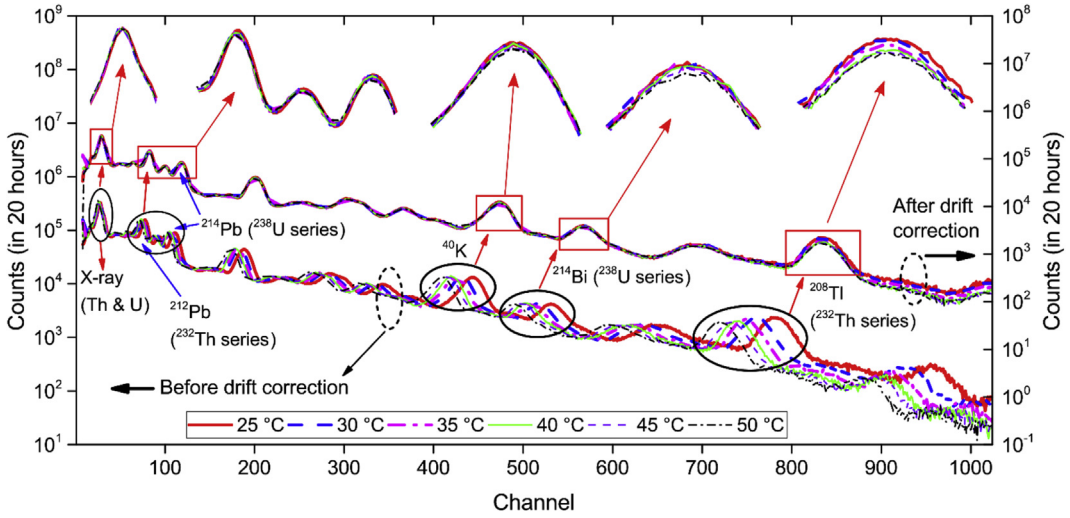

Fig. 5. Gamma spectra measured from the mixed ^{40}K, ^{238}U and ^{232}Th reference sample at temperatures between 25 °C and 50 °C, before (bottom group of spectra, left y axis) and after (top group of spectra, right y axis) drift correction. Enlarged insets shown at the top of the figure illustrate the accuracy of the correction for all peaks of interest.

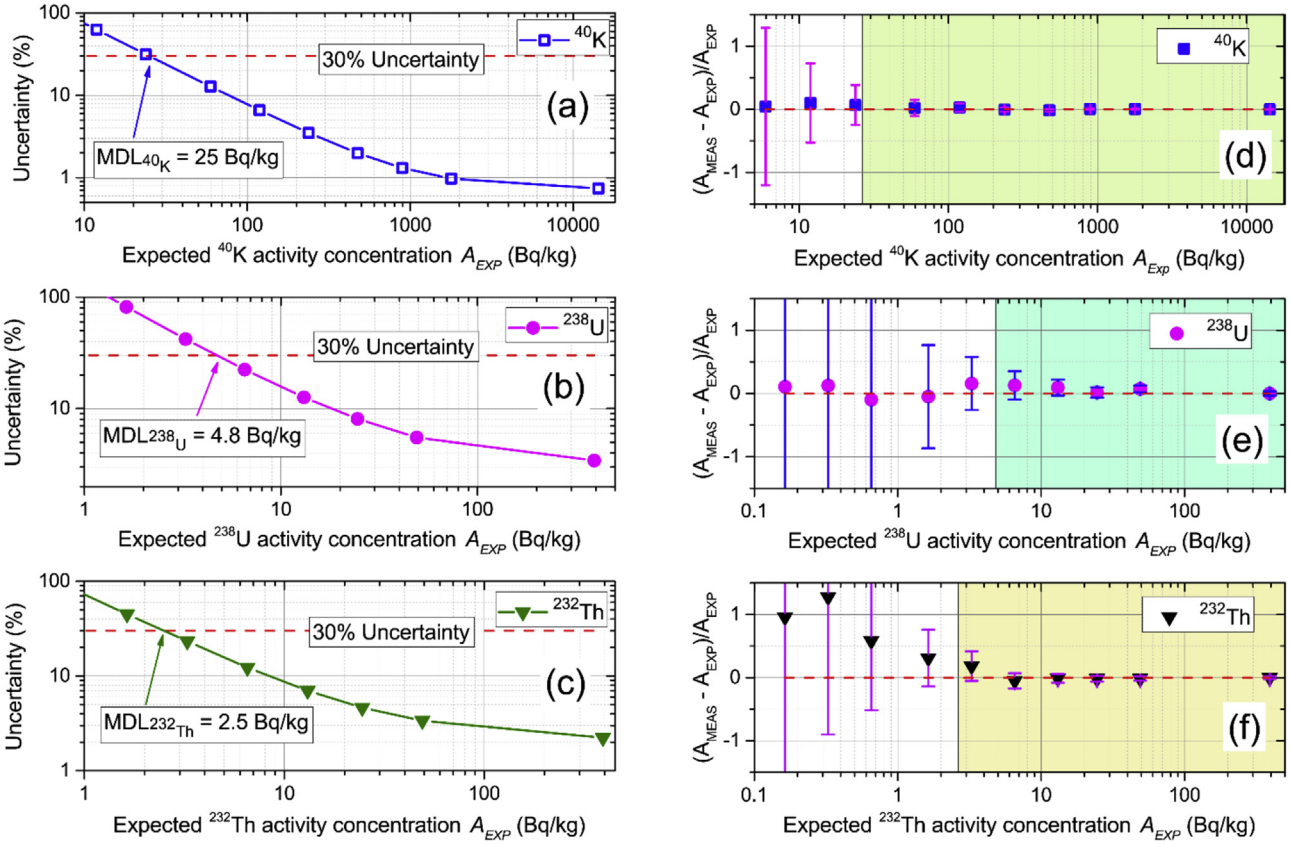

Fig. 6. (a–c) Variation of uncertainty with expected activity concentration (A_{EXP}), showing MDL (defined as measurement uncertainty of 30%) for ^{40}K, ^{238}U and ^{232}Th, respectively. (d–f) Comparison of measured ^{40}K, ^{238}U and ^{232}Th activity concentration (A_{MEAS}) and expected activity concentration (A_{EXP}).

$$C_{cK} = \begin{bmatrix} K_K \\ K_U \\ K_{Th} \end{bmatrix} = \begin{bmatrix} (K1_K + K2_K + K3_K)/3 \\ (K1_U + K2_U + K3_U)/3 \\ (K1_{Th} + K2_{Th} + K3_{Th})/3 \end{bmatrix}, \quad (8)$$

and the corresponding counting uncertainties are:

$$\begin{bmatrix} Un\_K_K \\ Un\_K_U \\ Un\_K_{Th} \end{bmatrix} = \begin{bmatrix} (\sqrt{Un\_K1_K^2 + Un\_K2_K^2 + Un\_K3_K^2})/3 \\ (\sqrt{Un\_K1_U^2 + Un\_K2_U^2 + Un\_K3_U^2})/3 \\ (\sqrt{Un\_K1_{Th}^2 + Un\_K2_{Th}^2 + Un\_K3_{Th}^2})/3 \end{bmatrix} \quad (9)$$

The uncertainty related to the ^{40}K, i.e., Un_C_{cK} includes the

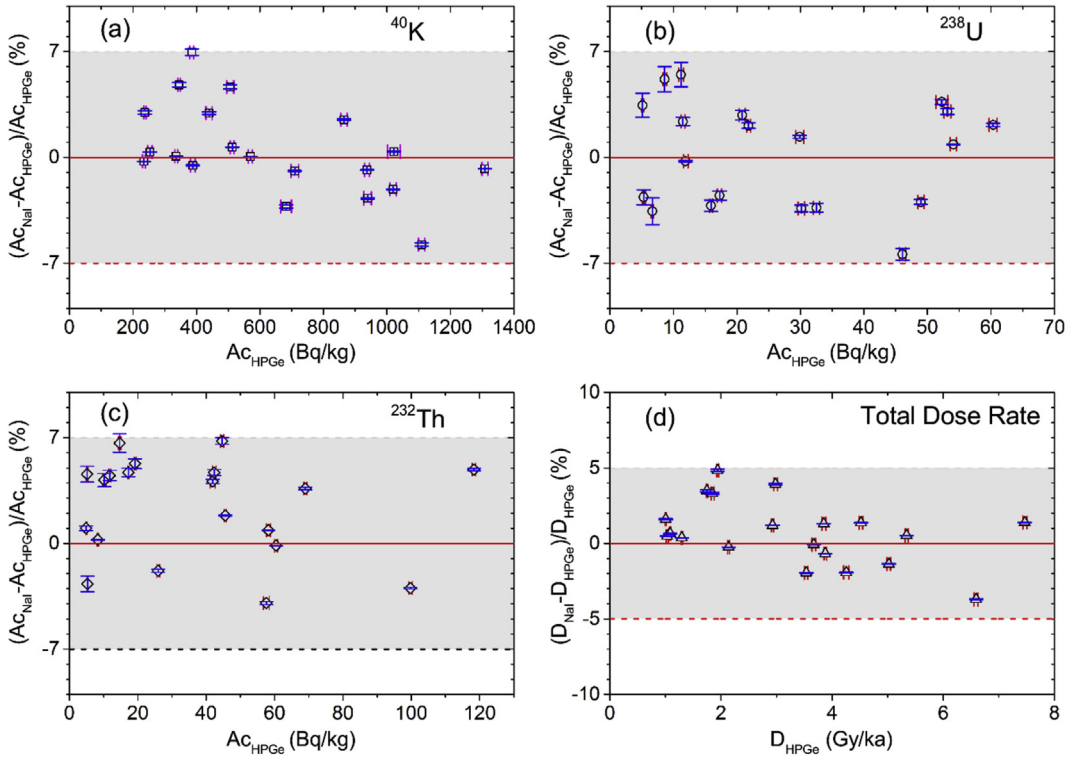

Fig. 7. Normalized deviations between ^{40}K, ^{238}U and ^{232}Th activity concentrations (a–c), and total (β plus γ) dose rates (d) determined by the NaI(Tl) spectrometer and expected values from an HPGe spectrometer, for a range of geological samples. The shaded areas in panels (a–c) are drawn at ± 7%, and in (d) at ± 5%.

counting uncertainty and the original material manufacturer's uncertainty Un_M_K (0.40% for ^{40}K), therefore:

$$Un\_C_{cK} = \begin{bmatrix} \sqrt{Un\_K_K^2 + Un\_M_K^2} \\ \sqrt{Un\_K_U^2 + Un\_M_K^2} \\ \sqrt{Un\_K_{Th}^2 + Un\_M_K^2} \end{bmatrix} \quad (10)$$

The same procedure was applied also to U1-3 and Th1-3 to obtain averaged coefficients C_{cU} and C_{cTh}, and their corresponding uncertainties Un_C_{cU} and Un_C_{cTh}, respectively (the manufacturer's relative uncertainties are 0.21% and 1% for ^{238}U and ^{232}Th, respectively). The averaged coefficients in the *Cc* matrix and their uncertainties in the *Un_Cc* matrix, together with the background count rates for our detector are summarised in the supplementary Table S1.

Knowing *Cc*, one can calculate the activity concentrations *Ac* in an unknown sample by solving the linear equation:

$$S = Cc \times Ac \quad (11)$$

Where $S = \begin{bmatrix} S_K \\ S_U \\ S_{Th} \end{bmatrix}$ is the array of total counts in ^{40}K, ^{238}U and ^{232}Th energy windows of sample spectrum after subtracting the background, and $Ac = \begin{bmatrix} Ac_K \\ Ac_U \\ Ac_{Th} \end{bmatrix}$ is the array of ^{40}K, ^{238}U and ^{232}Th activity concentrations contained in the unknown sample. The uncertainties of the ^{40}K, ^{238}U and ^{232}Th activity concentrations were also calculated during solving the linear equation (11) by the in-house developed DoseRateAnalyzer software.

3.3. Minimum detection limit (MDL)

Minimum detection limits for ^{40}K, ^{238}U and ^{232}Th activity concentrations are one of the most important specifications of a gamma spectrometer intended for measuring dose rates in dating applications. To measure these experimentally, the active mixed standard (containing ~2700 Bq ^{40}K, ~70 Bq ^{238}U and ^{232}Th) was first counted for various lengths of time *t*, of 30, 60, 120, 300, 600, 1200, 2400, 4500, 9000 and 72000 s, all at room temperature. These spectra were saved individually. Secondly, the background cup was counted for 72000, 71970, 71940, 71880, 71700, 71400, 70800, 69600, 67500, 63000 s, all at room temperature, and the spectra saved. All 20 spectra were then corrected for drift before one sample spectrum (e.g. 30 s) and the corresponding background spectrum (e.g. 71970 s) were summed to give a total counting time of 20 h (72000 s). This gave us a series of spectra equivalent to those that would have been obtained from a series of samples of well-known relative activity concentrations, all counted for 20 h. The expected activity concentration (A_{EXP}) corresponding to the counting time *t* of each simulated sample was calculated from the activity concentration measured for 20 h (A_{MEAS_20}).

$$A_{EXP} = A_{MEAS\_20} \times \frac{t}{72000} \quad (12)$$

The combined spectra were analysed as described above and the analyses summarised in Fig. 6(a–f). For simplicity, we define the MDL as the value of A_{EXP} expected to have a corresponding uncertainty of 30%. Based on Fig. 6(a–c), the MDLs for ^{40}K, ^{238}U and ^{232}Th are 25, 4.8 and 2.5 Bq/kg, respectively; especially for ^{40}K, these concentrations lie well below those found in most sediments.

Fig. 6(d–f) examines the accuracy of the analyses as the activity concentrations approach the MDLs, by presenting the deviations ($A_{MEAS} - A_{EXP}$) between the measured and expected activity concentrations for ^{40}K, ^{238}U and ^{232}Th. This deviation is then normalized to the expected activity concentration as $\frac{A_{MEAS} - A_{EXP}}{A_{EXP}}$ for easier comparison, and shown as a function of A_{EXP}. The shaded area in each subpanel of Fig. 6(d–f) indicates the activity concentration range above the MDL of ^{40}K, ^{238}U and ^{232}Th, as appropriate. Within these regions, ^{40}K, ^{238}U and ^{232}Th analyses all remain accurate, within 1σ of the expected result.

3.4. Activity concentration and dose rate determination in geological samples

Finally we evaluate the performance of our spectrometer, and the accuracy of the algorithm used to calculate the activity concentration of unknown samples, by comparison of our analyses with those from a high resolution facility (Murray et al. these proceedings), over a range of activity concentrations (Fig. 7(a–c)); the resulting dry dose rates are compared in Fig. 7(d). All unknown samples, ^{40}K, ^{238}U and ^{232}Th calibration standard cups, mixed ^{40}K, ^{238}U and ^{232}Th drift correction reference cup and background cup were measured at a room temperature of ~25 °C, without any temperature control. The maximum temperature drift during each measurement is ~0.4 °C. The background counts were subtracted from every measured sample spectrum, before the activity concentrations of ^{40}K, ^{238}U and ^{232}Th in each geological sample were calculated. As shown in Fig. 7(d), there is no suggestion of a systematic discrepancy in the total dry beta and gamma dose rates, and the average ratio of the dose rate determined on the NaI(Tl) system to that from the high resolution facility is 1.007 ± 0.005 (n = 20). The average relative random uncertainty on dose rates derived from the NaI (Tl) spectrometer is 1.3%, comparable with the 0.9% from the high resolution facility.

4. Conclusions

We have investigated the performance of a low cost, low maintenance laboratory spectrometry system based on a 3″×3″ NaI(Tl) crystal when determining burial dose rates in trapped charge dating. Gain drift is a potential problem, but this can readily be compensated for using a simple two-point correction algorithm. The MDLs for ^{40}K, ^{238}U, and ^{232}Th are all less than typical activities found in most dating samples, and comparison of analyses of unknown samples with those from our high resolution facility are very satisfactory. The average ratio of dose rates measured on our NaI(Tl) scintillation spectrometer to those from HPGe spectrometry is 1.007 ± 0.005 (n = 20), and the typical relative random uncertainties in dose rate of 1.3% are comparable with those from high resolution spectrometry. We conclude that the new scintillation spectrometry system is a useful alternative laboratory method for determining dose rate at a significantly lower cost than high resolution spectrometry. This, combined with the large (and so more representative) sample size makes it a strong competitor to other analytical methods used in dating.

Acknowledgements

J.-P. Buylaert received funding from the European Research Council under the European Union Horizon 2020 research and innovation programme (grant number: ERC-2014-StG 639904 – RELOS).

Appendix A. Supplementary data

Supplementary data related to this article can be found at https://doi.org/10.1016/j.radmeas.2018.07.003.

References

Borg, P.J., Huppert, P., Phillips, P.L., Waddington, P.J., 1985. A microprocessor-based gamma-ray spectrometer with gain stabilized single-channel analyzers. Nucl. Instrum. Meth. Phys. Res. A 238, 104–110.

Casanovas, R., Morant, J.J., Salvado, M., 2012. Temperature peak-shift correction methods for NaI(Tl) and $LaBr_3$(Ce) gamma-ray spectrum stabilisation. Radiat. Meas. 47, 588–595.

Desbarats, A.J., Killeen, P.G., 1990. A least-squares inversion approach to stripping in gamma-ray spectral logging. Nucl. Geophys. 4 (3), 343–352.

Marett, G., Chevalier, P., Souhaite, P., Suau, J., 1976. Shaly sand evaluation using gamma ray spectrometry applied to the North Sea Jurassic. In: Soc. Professional Well Log Analysts (SPWLA), 17th Ann. Logging Symposium Trans. Denver, Colorado.

Mitra, P., Roy, A.S., Verma, A.K., Pant, A.D., Prakasha, M.S., Anilkumar, S., Kumar, A.V., 2016. Application of spectrum shifting methodology to restore NaI(Tl)-recorded gamma spectra, shifted due to temperature variations in the environment. Appl. Radiat. Isot. 107, 133–137.

Moszynski, M., Nassalski, A., Syntfeld-Kazuch, A., Szczesniak, T., Czarnacki, W., Wolski, D., Pausch, G., Stein, J., 2006. Temperature dependences of $LaBr_3$(Ce), $LaCl_3$(Ce) and NaI(Tl) scintillators. Nucl. Instrum. Meth. Phys. Res. A 568, 739–751.

Murray, A.S., Buylaert, J.-P., Thiel, C., 2015. A luminescence dating intercomparison based on a Danish beach-ridge sand. Radiat. Meas. 81, 32–38.

Murray, A.S., Helsted, L.M., Autzen, M., Jain, M., Buylaert, J.-P., 2018. Measurement of natural radioactivity: calibration and performance of a high-resolution gamma spectrometry facility. Radiat. Meas. https://doi.org/10.1016/j.radmeas.2018.04.006 (in press).

NRCAN-1, Uranium Ore BL-5, Natural Resources Canada, http://www.nrcan.gc.ca/mining-materials/certified-reference-materials/certificate-price-list/8115.

NRCAN-2, Thorium Ore OKA-2, Natural Resources Canada, http://www.nrcan.gc.ca/mining-materials/certified-reference-materials/certificate-price-list/8135.

Plettner, C., Scherwinski, F., Pausch, G., Lentering, R., Kong, Y., Stein, J., 2011. Anomalous gain drop effects in Hamamatsu 3998-01 photomultiplier. In: IEEE Conference Record - Nuclear Science Symposium and Medical Imaging Conference, pp. 1634–1637.

Qin, Z., Ge, L., Wu, Q., Cheng, J., 2012. A new algorithm for spectral drift calculation in a gamma-ray spectrometer. Adv. Mater. Res. 346, 705–710.